File

INTERNAL DOCUMENT 97

I.O.S.

THE EVALUATION OF WAVE REFRACTION CALCULATIONS USING OBSERVED WAVE DATA

by

H L KING and P J HARDCASTLE

NATURAL ENVIRONMENT RESEARCH COUNCIL
INSTITUTE OF OCEANOGRAPHIC SCIENCES

INSTITUTE OF OCEANOGRAPHIC SCIENCES

Wormley, Godalming,
Surrey, GU8 5UB.
(042-879-4141)

(Director: Dr. A. S. Laughton)

Bidston Observatory,
Birkenhead,
Merseyside, L43 7RA.
(051-652-2396)
(Assistant Director: Dr. D. E. Cartwright)

Crossway,
Taunton,
Somerset, TA1 2DW.
(0823-86211)
(Assistant Director: M.J. Tucker)

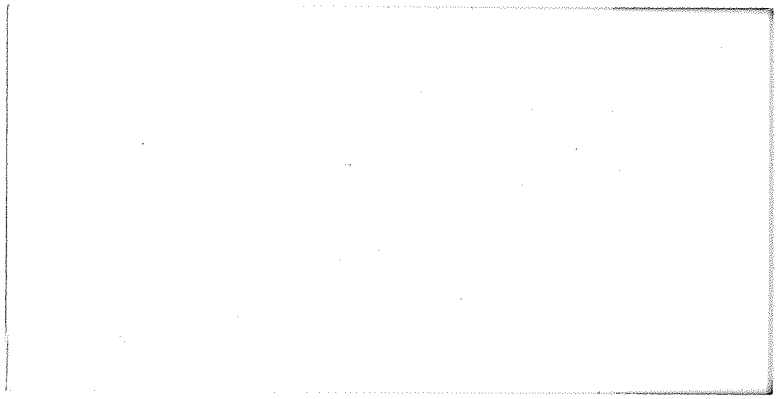

THE EVALUATION OF WAVE REFRACTION CALCULATIONS USING OBSERVED WAVE DATA

by

H L KING and P J HARDCASTLE

INTERNAL DOCUMENT NO 97

Institute of Oceanographic Sciences
Crossway
Taunton
Somerset
TA1 2DW

June 1980

EDITORIAL NOTE

This Report is in the nature of a discussion document and comments will be welcomed. It describes the work so far undertaken at the Institute of Oceanographic Sciences and points the way to further research.

IOS is very aware of the limitations of the work reported here. In particular the data are from only one location and represent a limited range of wave conditions. The results indicate that while the wave refraction technique is valuable for predicting inshore wave climates, there are certain aspects which require further investigation.

1. INTRODUCTION

Calculations based on linear wave theory can be used to predict inshore wave climates from the corresponding measured or predicted offshore climate (eg Abernethy and Gilbert, 1974). The calculations make certain assumptions so that they are practicable in terms of run-time and cost. For example:

(a) The seabed topography is approximated by a mesh of finite size which excludes the small scale features.
(b) The energy loss through breaking waves and bottom and surface stress is neglected.

As far as the authors are aware there has been no extensive check as to whether the inshore wave climates, as predicted by such calculations, agree with observed measurements. At Start Bay, Devon, relevant field information could be obtained from equipment already deployed as part of a multi-disciplinary research programme in the area. (Some results of this programme were published in the Journal of the Geological Society, 1975, Vol 131, Part 1). The opportunity was therefore taken to validate the refraction calculations with these data. The methods and results of the comparison are reported below.

2. FIELD DATA: INSTRUMENTATION AND PROCESSING

A map of the area, with the relevant locations marked, is given as Figure 1.

A range of wave recording instruments were used to collect data from mid-February to the end of May 1974. The remote recording pressure unit at Redlap Cove (labelled 4 in Fig 1) did not provide sufficient data for this report. The three FM pressure recorders at Hallsands (Target 1), Beesands (Target 2) and Slapton Monument (Target 3) were cabled to the shore and provided data for this study. Concurrently a Waverider buoy was installed near the Bell Buoy, just offshore of the Skerries.

All the wave data were recorded using frequency modulation on magnetic tape. The recordings were of 1350 seconds duration and taken at intervals of 3 hours. These were replayed to give significant wave height $H_{\frac{1}{3}}$ (from mean rectified wave height) and the mean zero crossing period T_z. It should be mentioned that due to the attenuation of pressure variation with depth, the pressure recorders respond less to short period waves than the Waverider buoy. To reduce this discrepancy, appropriate correction factors were calculated from an empirical attenuation formula (Draper, 1957), using the actual depth and measured T_z. These values varied slightly about 1.9 and were applied directly to the $H_{\frac{1}{3}}$ values.

Information about the wave directions was obtained from pictures, taken every three hours, of a 3cm X-band radar display mounted at Tor Cross (Fig 1).

Although all the data are available in a form that can give actual power spectra with a Fast Fourier Transform (FFT), the FFT spectral form was not used for the computations discussed here. However, a comparison between FFT spectra and the theoretical form used, is shown in Figure 7. It is hoped to use measured spectra in future work. The recorders at Hallsands and Slapton Monument were maintained in operation after the experimental period, since the wave refraction diagrams produced by Dr (now Professor) P Holmes at Liverpool University (Holmes, 1975) showed a focussing effect on Hallsands for waves with an easterly component. It was hoped to obtain experimental justification for this prediction during severe easterly conditions.

3. SUMMARY OF THE COMPUTATIONAL METHODS USED FOR THE WAVE REFRACTION PREDICTIONS.

The details of the theory behind the computations are given in Appendix 1.

The method used was that developed by the Hydraulics Research Station (HRS) of the Department of the Environment (HRS, 1974). The subroutines required for the ray path-tracking were obtained directly from HRS listings while the rest of the computations were developed from the appendices of the HRS report.

The computations are done in three stages:

(a) Firstly, the seabed topography information is used to determine transfer functions for the directional wave spectrum $S(f,\theta)$ for each target point. All notation is defined in Appendix 1.

Starting at a target point ray paths are tracked outwards for a discrete set of equally spaced frequencies. The rays are started at equally spaced angular increments suitable for the frequency. HRS found that it was possible to use larger increments for the upper end of their frequency band than for the lower (see HRS, 1974). The rays halt at 'obstacles' or on the grid boundary. Since the paths are reversible, only the rays which reach the deep-water boundary are of interest, but their exact position is immaterial since the spectrum is assumed constant along the deep water boundary.

Longuet-Higgins (1957) has shown that $c\,c_g\,S(f,\theta)$ is constant along a ray path, whence it is possible to calculate the transfer functions to obtain the inshore frequency spectrum from the offshore directional spectrum (see Appendix 1).

(b) An offshore ('deep-water') directional spectrum can be determined from measured wave data either by assuming some form of distribution for both frequency and direction, or the frequency distribution form may be replaced by a frequency spectrum obtained directly from the wave data (see Appendix 2).

A modified Pierson-Moskowitz spectrum (HRS, 1974, and Pierson et al, 1974) was used to approximate the frequency spectrum in this study, although some preliminary work on FFT spectra is also incorporated (Figure 7).

The offshore spectral matrix is pbtained by evaluating the directional spectrum at each frequency and angular segment. These segments are distinct from the angular increments mention in 3(a), and may be several

orders of magnitude larger. The segment size is chosen so that $S(f,\theta)$ is approximately independent of θ in each segment.

(c) The inshore predictions of significant wave height and mean zero crossing period can be calculated from the inshore frequency spectrum for each target point (see Appendix 1).

4. INPUT DATA USED FOR THE COMPUTATIONS AND DESCRIPTION OF THE MEASURED PARAMETERS

For the energy transfer function calculations the sea bed topography was described by depth values taken from the Admiralty fair sheet (Aston and Gratton, 1951). Each grid point was assigned the depth value closest to it. The dimensions of the whole grid were 25 points roughly parallel to the shore and 18 points offshore with a mesh size of 463 x 463 metres (Fig.1). The offshore angular segment size was taken as 20°, since this is the order of accuracy of measuring wave directions. The frequency bandwidth was defined by discrete frequencies at 0.02 Hz intervals from 0.05 Hz to 0.25 Hz. This choice was made and the computations for this report done before any offshore wave records were spectrally analysed. The spectra suggest that an upper limit of 0.03 or 0.04 Hz should be used in future computations. The choice of angular ray separation, inshore, was suggested by the HRS report, (HRS, 1974), namely $\frac{1}{2}^{\circ}$ for 0.05 to 0.15 Hz and $\frac{3}{4}^{\circ}$ for 0.17 to 0.25 Hz. The functions were calculated for each water level above chart datum that corresponded with the water depths associated with the observed wave parameters. In order to obtain predicted inshore values of $H_{1/3}$ and T_z that could be compared with observed values, the corresponding offshore wave climate, in terms of $H_{1/3}$, T_z and mean direction, was required. The $H_{1/3}$ and T_z values used were those obtained from the Waverider data and the mean offshore direction was estimated by the angle of wave approach indicated by the radar information (see Section 2).

The data, so obtained, produced a total of 201 comparable observations of both $H_{1/3}$ and T_z. These were sorted by three factors.

(i) Water depth above chart datum which gave 9 groups of between 7 and 34 observations.

(ii) Target points which gave 56 observations for targets 1 and 2, and 89 for target 3.

(iii) Offshore direction which gave 155 observations for waves from a direction less than 120°N and 46 for directions greater than 120°N.*

*All bearings are true

Before proceeding with the comparison of the observed and predicted inshore wave climates, the observed offshore and inshore data are briefly described.

The mean $H_{1/3}$ and T_z for various groups of the data are given below:

	Data	Mean $H_{1/3}$	Mean T_z
Offshore Data	All	1.03m	5.7s
	from directions $\leqslant 120^{\circ}N$	0.91m	5.6s
	from directions $> 120^{\circ}N$	1.30m	6.2s
Inshore Data	All	0.79m	6.6s
	for offshore directions $\leqslant 120^{\circ}N$	0.81m	6.2s
	for offshore directions $> 120^{\circ}N$	0.73m	7.8s
	At target 1 - Hallsands	0.79m	6.3s
	At target 2 - Beesands	0.74m	6.5s
	At target 3 - Slapton	0.83m	6.8s

The ranges of $H_{1/3}$ and T_z were found to be respectively

for offshore data: 0.03 - 2.37m ; 4.5 - 7.6s

for inshore data: 0.06 - 1.92m ; 5.1 - 12.8s.

The waves approached from directions between $70^{\circ}N$ and $170^{\circ}N$. Those from bearings greater than $120^{\circ}N$ tended to have larger values of both $H_{1/3}$ and T_z than waves from other directions. According to the wave data the waves lost height and increased their period as they travelled inshore. This maybe an effect of the difference in the instrumentation used to measure the inshore and offshore conditions, but at present, there is no better correction factor for pressure recorders available.

The mean values of the observed $H_{1/3}$ and T_z were calculated for each water level and plotted as part of figure 2. The mean inshore $H_{1/3}$ did not vary significantly with water level, although there was a tendency for lower values for the lowest and highest water levels. This tendency was more definite for the offshore $H_{1/3}$. For the T_z values, the offshore means were reasonably constant with respect to water level, whereas the inshore values definitely peaked at about 2.5m above chart datum.

These are strictly observations, further analysis and conclusions are outside the aims of this report.

5. RESULTS

The predicted and observed values of $H_{1/3}$ and T_z were compared using graphical and statistical methods. Their agreement was found to depend on

(a) the inshore location
(b) the mean offshore wave direction
(c) the combination of (a) and (b)
(d) the water level above chart datum, namely the tide height.

The mean values for each water level (d) calculated from the values at all locations were plotted (see Fig. 2). The means of the observed and predicted inshore $H_{1/3}$ agree reasonably well at all water levels. For T_z, the predicted values peak, as do the observed T_z, but at a higher water level of 3.3m above chart datum.

The mean values of $H_{1/3}$ and T_z at each target point are given below:

		$H_{1/3}$	T_z
Offshore observations		1.03m	5.7s
Target 1	Observed	.79m	6.3s
	Predicted	.66m	6.6s
Target 2	Observed	.74m	6.5s
	Predicted	.95m	6.8s
Target 3	Observed	.83m	6.8s
	Predicted	.78m	6.8s

With the hope of finding trends, the predictions and observations were compared in variously sorted groups provided that there was a sufficient number of observations within the group to allow significant statistical comparison. Two statistical tests were applied: (i) comparison of paired samples using Student's t distribution (Snedecor et al, 1967), and (ii) a Kendall and Stuart test (Kendall et al, 1975), as to whether two random samples come from identical populations. The tests were repeated for the T_z values neglecting

any pairs whose observed values were greater than or equal to 9.0s. The graphs of predicted versus observed T_z shown in Figures 3 - 6 indicated that these large observed values might be 'rogue'.

The results of the statistical tests agreed well with each other and a visual assessment of the graphs. Some of the results of the paired sample comparison test are given in Table 1.

Considering all the data as a single group, the predicted $H_{1/3}$ compared very well with the observed values at the 0.05 significance level. For T_z , however, the predictions were greater than the observed values at the same level of significance. The mean value of this difference was 0.14s when using all T_z values and 0.33s when T_z greater than 9.0s were neglected.

The data then considered in groups according to (a) inshore target location, or (b) mean offshore wave direction. There were insufficient data to warrant analysis of the groups selected by both (a) and (b) together. From Table 1, the predictions of T_z appeared to be high, except when compared with the 'rogue' values which are all associated with waves from a SSE direction. For $H_{1/3}$, agreement between the predicted and observed values depended on the grouping categories. This dependance suggests that either or both of the grid system and the offshore boundary are inadequately described for the computations.

Using the maximum mean deviations in Table 1 the difference between the predicted and observed values represented about 20% and 10% of the mean observed $H_{1/3}$ and T_z respectively.

CONCLUSIONS

The mthod described seems adequate for first order estimates of inshore $H_{1/3}$ and T_z. The main emphasis should be placed on the $H_{1/3}$ comparison because, for example, observed T_z may be considerably affected by the instrumental characteristics of the wave recorders. It is realised that the quantity and range of wave data used in this study are limited, especially for waves from the SSE.

Consideration of the theory and approximations involved in the computations imply that the deviations could be influenced by the following:

(a) the assumptions made in the theory may not represent the situation adequately. For example, surface and bottom stress or tidal currents may have significant effect on refraction. Also a uniform offshore energy spectrum may not be a reasonable assumption on the offshore boundary used.

(b) An inadequate depth grid approximation. Either the overall area may be too small with a poorly represented offshore boundary or the grid interval may be too large to define the sea-bed topography adequately.

(c) A poor choice for the particular area of some of the input parameters to the computations, for example, frequency band width and inshore angular increment.

(d) The Pierson-Moskowitz spectrum may give poor estimates of the spectral matrices of the offshore wave conditions.

The significance of the variation caused by factors (b) and (c) should be studied using the predictions obtained from the computations using different depth grid approximations and input parameters. For example, the grid area could be usefully extended further south from Start Point. The offshore boundary region would then include more wave energy from a southerly direction. Also a smaller grid interval should be considered, to improve the definition of the sea-bed.

The effects of the use of the Pierson-Moskowitz spectrum (d) could be investigated by using other approximations (e.g. JONSWAP). However, it would be preferable to

use a frequency spectrum obtained directly from the offshore wave data. Examples of the differences between the Pierson-Moskowitz and observed spectra are illustrated in Figure 7. For the directional aspect, however, present techniques provide no other means of representation than by assuming a standard form.

Before these computations can be considered to be adequately assessed they should be validated for locations with bathymetry and wave periods different from those in Start Bay. This is an immediate proposition because sufficient raw data from two other locations are already available.

7. REFERENCES

Abernethy, C. L., and Gilbert, G., 1974. "Refraction of a wave spectrum". Hydraulics Research Station. INT 117.

Cartwright, D. E., and Longuet-Higgins, M. S., 1956. "The statistical distribution of the maxima of a random function". Proc. Roy. Soc. A. 237, pp. 212-232.

Draper, L., 1957. "Attenuation of sea waves with depth". La Houille Blanche 12 pp. 926-931.

Hasselmann, K., et al, 1973. "Measurements of wind wave growth and swell decay during the Joint North Sea Wave Project (JONSWAP)". Deutches Hydrographisches Institut Reihe A (8°) Nr. 12.

Holmes, P. K., 1975. "Wave conditions in Start Bay". Jl. Geol. Soc. 131, pp. 57-62.

Hydraulics Research Station, 1974. "Maplin investigations : a wave refraction study in the Thames estuary". Report EX 659.

Kendall, M. G., and Stuart, A., 1973. "The advanced theory of statistics". Vol. 2 "Interference and Relationship". 3rd edition. Griffin. pp. 505-509.

Longuet-Higgins, M. S., 1957. "On the transformation of a continuous spectrum by refraction". Proc. Camb. Phil. Soc. 53 pp. 226-229.

Pierson, W. J. Jr., and Moskowitz, L., 1964. "A proposed spectral form for fully developed seas based on the Similarity Theory of S. H. Kitaignodskii". Jl. Geophys. Res. 69. pp. 5181-5190.

Snedecor, G. W., and Cochran, W. G., 1967. "Statistical methods". 6th edition, Iowa State University Press. pp. 91-96.

APPENDIX 1

1. Ray Tracking

The sea-bed is defined over a rectangular set of grid points. A diagonal across each rectangle defines a system of triangles. The standard linear wave theory gives the relationship $\sigma c = g \tan h \frac{\sigma h}{c}$

where σ = radian frequency
c = phase velocity (celerity)
h = water depth
g = acceleration due to gravity

Thus the celerity can be calculated at all grid points and can be interpolated over each triangle by the formula $c = px + qy + r$

where p, q, r are constants.

Furthermore this formula will be continuous across all triangle boundaries.

Using Snell's Law and this linear representation of c it can be shown that the ray path through the triangle is an arc of a circle.

Thus given a wave frequency and initial direction, a wave ray can be tracked from any starting point within the grid area, triangle by triangle, until it reaches an end point.

2. Energy Transfer Functions

Let the directional wave spectrum be defined by $S(f, \Theta)$ where f is angular frequency and Θ is direction.

It can be shown (Longuet-Higgins, 1957) that making certain assumptions

$S(k_1, k_2)$ = constant along a wave ray path

where $\underline{k} = (k_1, k_2)$ is a two dimensional wave number.

Transforming the spectrum to (f, Θ) co-ordinate system to maintain volume elements of energy

$$S(f, \Theta)\, df\, d\Theta = S(k_1, k_2)\, dk_1\, dk_2$$

whence

$$S(k_1, k_2) = S(f, \Theta) \frac{df}{dk_1} \frac{d\Theta}{dk_2}$$

$$= S(f, \Theta) \frac{1}{k} \frac{df}{dk} \qquad \text{since } dk_1\, dk_2 = k\, dk\, d\Theta$$

where $k = |\underline{k}|$

$$= \frac{c}{f}\, c_g\, S(f, \Theta)$$ where c_g is group velocity

c is phase velocity

Thus $cc_g\, S(f, \Theta)$ is constant along a ray path whenever f is constant.

Define $S_i(f, \Theta_i)$ as the inshore spectrum and $S_o(f, \Theta_o)$ as the offshore one.

Then $(cc_g)_i\, S_i(f, \Theta_i) = (cc_g)_o\, S_o(f, \Theta_o)$

$$S_i(f, \Theta_i) = \mu(f)\, S_o(f, \Theta_o)$$

where $$\mu(f) = \frac{(cc_g)_o}{(cc_g)_i}$$

To obtain inshore values for $H_{1/3}$, T_z $S_i(f)$ is required

where $$S_i(f) = \int_{\Theta_i \in \Omega} S_i(f, \Theta_i)\, d\Theta_i$$

$$= \mu(f) \int_{\Theta_i \in \Omega} S_o(f, \Theta_o) d\Theta_i$$

and Ω is the angular range of interest at the target point.

Assuming that $S_o(f, \Theta_o)$ is sufficiently smooth

$$S_o(f, \Theta_o) = \sum_{n=1}^{N} \frac{A_n(f)}{\Delta_o \Theta} H(\Theta - n * \Delta_o \Theta)$$

where $\Delta_o \Theta$ is the angular segment of the offshore direction

N is the number of such segments

$A_n(f)$ is the total energy for frequency f in directional segment n.
(i.e. $\Theta_o \in [n\Delta_o\Theta, (n+1)\Delta_o\Theta]$)

$$H(x) = \begin{cases} 1 & \text{if } 0 < x \leq \Delta_o\Theta \\ 0 & \text{otherwise} \end{cases}$$

Substituting for $S_o(f, \Theta_o)$ in the expression for $S_i(f)$ and approximating the integral by a summation over the numbers of rays arriving at the inshore target point (ray paths are reversed after tracking):

$$S_i(f) = \mu(f) \frac{\Delta_i \Theta}{\Delta_o \Theta} \sum_n N_n A_n(f) \underset{\text{defn.}}{=\!=} \sum_n A_n T_n$$

where $\Delta_i \Theta$ is the angle between rays arriving at the target point

N_n is the number of rays whose offshore direction θ_o is in the nth directional segment.

The inshore $H^1/_3$ and T_z can be calculated from the zero and second order moments of S(f) (Cartwright et al, 1956).

$$H_{1/3} = 4 M_o^{\frac{1}{2}} \qquad T_z = 2\pi (M_o/M_2)^{\frac{1}{2}}$$

where $M_o = \int_o^\infty S(f)\, df$ $\qquad M_2 = 4\pi^2 \int_o^\infty f^2 * S(f)\, df.$

For the computations the integrals are replaced by summations, assuming Δf is sufficiently small. To obtain an estimate of the mean inshore wave direction $\bar{\Theta}(f)$ the series approximation for $S_o(f, \Theta_o)$ is substituted in the definition of the mean vector $\bar{V}$ at the target point, namely

$$\bar{V} = \frac{\int_{\Theta_i \in \Omega} S_i(f, \Theta_i)\, e^{i\Theta_i}\, d\Theta_i}{\int_{\Theta_i \in \Omega} S_i(f, \Theta_i)\, d\Theta_i} .$$

Then $$\bar{\Theta}(f) = \tan^{-1} \sum_n A_n(f)\, V_n(f) \Big/ \sum_n A_n(f)\, U_n(f)$$

where $$U_n(f) + iV_n(f) = \mu(f) \frac{\Delta_i \Theta}{\Delta_o \Theta} \sum_{\text{rays in segment n.}} e^{i\Theta_i}$$

Thus the transfer functions T_n, U_n, V_n are calculated from

$$\begin{pmatrix} T_n \\ U_n \\ V_n \end{pmatrix}(f) = \mu(f) \frac{\Delta_i \Theta}{\Delta_o \Theta} \sum_{\substack{\text{rays in} \\ \text{segment} \\ n}} \begin{pmatrix} 1 \\ \cos \Theta_i \\ \sin \Theta_i \end{pmatrix}$$

for the set of frequencies $\{f_m : m = 1, \ldots . M\}$ and stored in a file as the matrix elements :

$$T_{nm} = T_n(f_m), \quad U_{nm} = U_n(f_m) \quad \text{and } V_{nm}(f_m).$$

Once these functions are available it is relatively fast calculation to determine $S_i(f_m)$ and $\overline{\Theta}(f_m)$ from the offshore spectral matrix $\{A_{nm} = A_n(f_m)\}$ (See Appendix 2).

APPENDIX 2

Offshore wave spectrum forms

The offshore values $\{A_{nm}\}$ can be estimated in a variety of ways. Since it is usually the frequency spectrum S(f) that is studied rather than S(f, Θ), the directional distribution is assumed.

$$S_o(f, \Theta) = S_o(f) * G(\Theta)$$

where $G(\Theta) = \frac{2}{\pi} \cos^2(\Theta - \Theta_M) \qquad |\Theta - \Theta_M| \leq \pi/2$

and Θ_M is the mean direction (Hasselmann et al, 1973)

Values of $S_o(f)$ can either be taken directly from a frequency spectral analysis of the offshore wave data, or can be estimated using a theoretical (empirical) approximation (e. g. Pierson-Moskowitz, JONSWAP).

Since the available offshore wave data was in the form of $H^1/_3$ and T_z values the approximation used for this comparison study was one derived from the Pierson-Moskowitz spectrum to include the parameters $H^1/_3$ and T_z.

$$S_o(f) = \frac{H_{\frac{1}{3}}^2}{4\pi T_z^4 f^5} * \exp\left[\frac{-1}{\pi (T_z f)^4}\right]$$

Thus the values $\{A_{nm}\}$ were calculated from the approximation

$$A_{n\,m} = A_n(f_m) = S_o(f_m) * G(\Theta_n) * \Delta_o\Theta$$

where Θ_n is the direction representative of the nth offshore directional segment.

TABLE 1

Paired Sample Comparison Test of Observed versus Predicted $H_{\frac{1}{3}}$ and T_z

Null Hypothesis $H_o : \mu_D = 0$

SIGNIFICANT WAVE HEIGHT $H_{1/3}$	n.p	DATA	MEAN ZERO CROSSING PERIOD T_z including $T_z \geqslant 9.0$s	n.p	MEAN ZERO CROSSING PERIOD T_z excluding $T_z \geqslant 9.0$s	n.p
Accept H_o Strongly	194	ALL	Reject H_o: pred > obs $\lvert\mu_D\rvert = 0.14$s $\lvert\mu_D\rvert \in (0.0, 0.28)$	194	Reject H_o: pred > obs $\lvert\mu_D\rvert = 0.33$s $\lvert\mu_D\rvert \in (0.23, 0.42)$	183
		Grouped by Location				
Reject H_o: obs > pred $\mu_D = 0.13$m $\mu_D \in (0.06,0.19)$	56	Target 1 Hallsands	Reject H_o: pred > obs $\lvert\mu_D\rvert = 0.35$s $\lvert\mu_D\rvert \in (0.14,0.55)$	56	Reject H_o: pred > obs $\lvert\mu_D\rvert = 0.31$s $\lvert\mu_D\rvert$ (0.12,0.50)	55
Reject H_o: pred > obs $\lvert\mu_D\rvert = 0.21$m $\lvert\mu_D\rvert \in (0.14,0.27)$	56	Target 2 Beesands	Cannot Reject H_o.	56	Reject H_o: pred > obs $\lvert\mu_D\rvert = 0.37$s $\lvert\mu_D\rvert \in (0.22,0.51)$	51
Cannot Reject H_o	89	Target 3 Slapton	Cannot Reject H_o.	89	Reject H_o: pred > obs $\lvert\mu_D\rvert = 0.31$s $\lvert\mu_D\rvert \in (0.16,0.45)$	78
		Grouped by direction				
Reject H_o: obs > pred $\mu_D = 0.06$m $\mu_D \in (0.01,0.10)$	155	Offshore direction $(70,120)^{\circ}$N (ENE - ESE)	Reject H_o pred > obs $\lvert\mu_D\rvert = 0.42$s $\lvert\mu_D\rvert \in (0.33,0.50)$	155	Reject H_o: pred > obs $\lvert\mu_D\rvert = 0.39$s $\lvert\mu_D\rvert \in (0.31,0.46$	149
Reject H_o: pred obs $\lvert\mu_D\rvert = 0.21$m $\lvert\mu_D\rvert \in (0.12,0.29)$	46	Offshore direction $(120,170)^{\circ}$N (SE - S)	Reject H_o: obs > pred $\mu_D = 0.64$s $\mu_D \in (0.15,1.12)$	46	Cannot Reject H_o.	34

Note A 95% confidence level was used to obtain these results.
For details of the method see Snedecor and Cochran (1967)

Notation
- n.p - The number of (obs - pred) pairs in the test
- μ_D - The mean of the populational deviations (obs - pred) values.
- $\lvert\mu_D\rvert$ - The absolute value of μ_D.
- $\mu_D \in [a,b]$ - means that $a \leq \mu_D \leq b$.

Figure 1 Location diagram

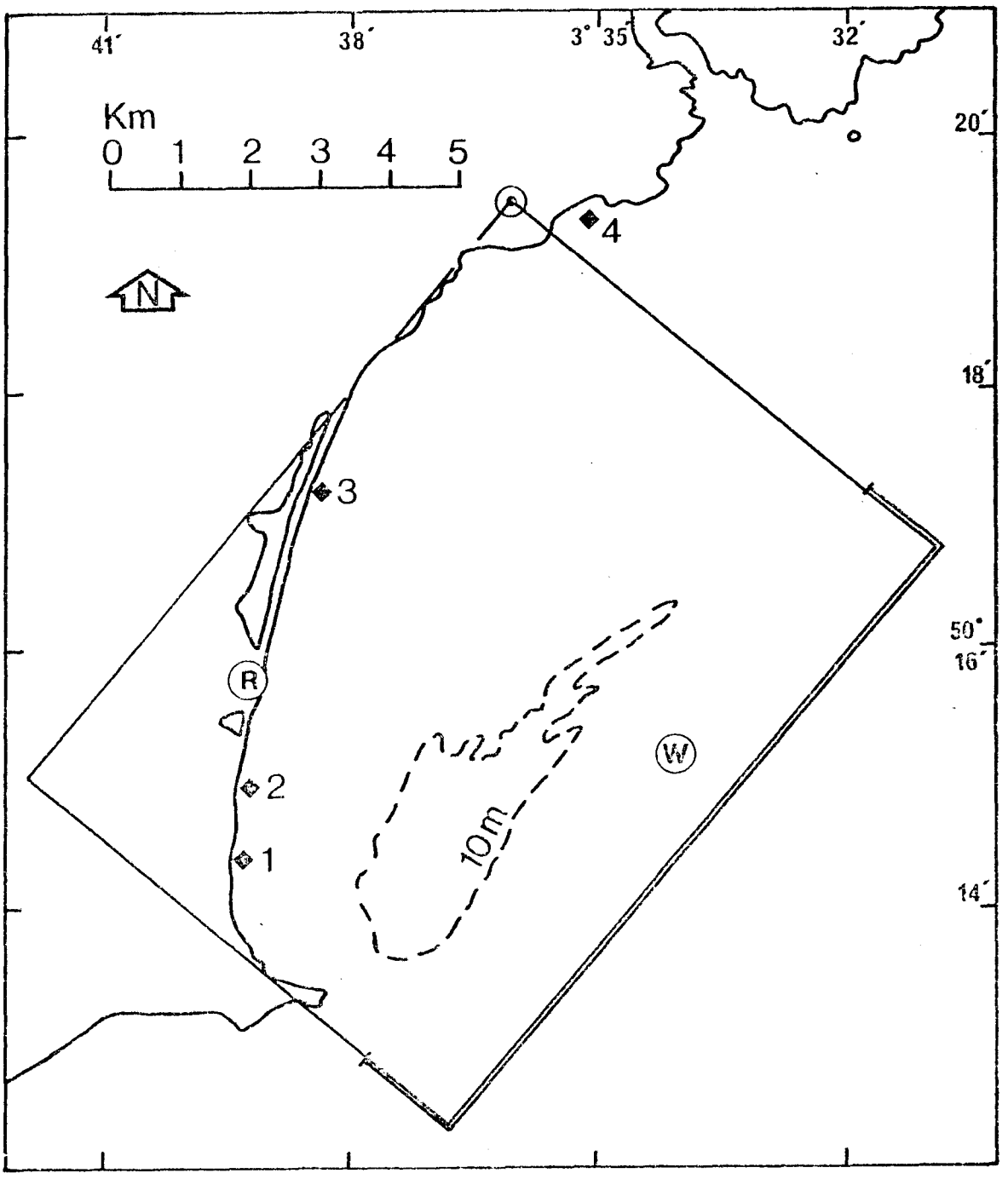

Key:

⊙ Geographical coords of origin: 50°19·6′N 3° 36·2′W

Grid Boundary

Section of boundary where waves are assumed to arrive.

◆ Inshore target points: 1. Hallsands
(pressure recorders) 2. Beesands
3. Slapton
4. Redlap Cove (not used in computations)

Ⓦ Offshore Wave Rider

Ⓡ Radar

Figure 2 Variation of mean $H_{\frac{1}{3}}$ and T_z with water depth

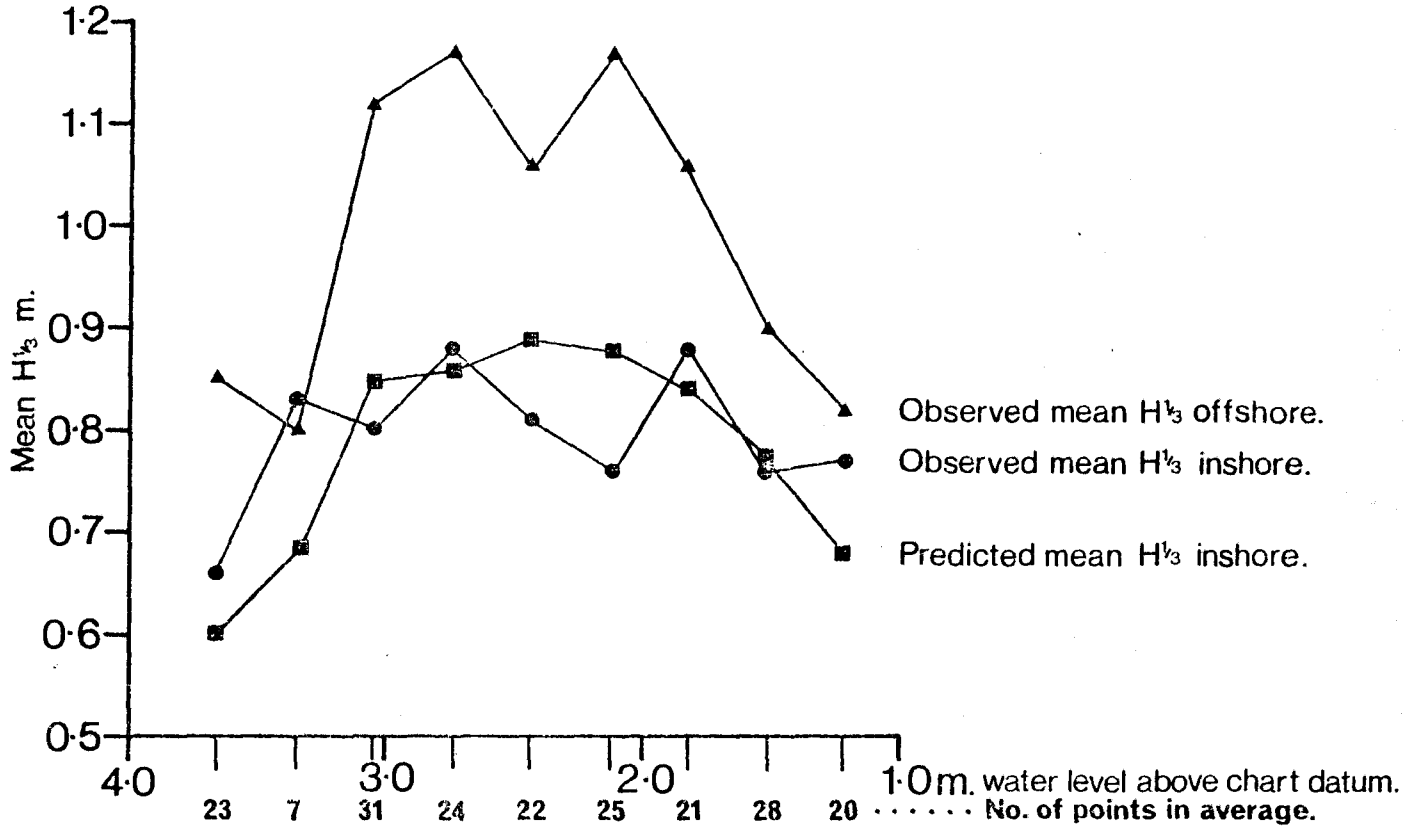

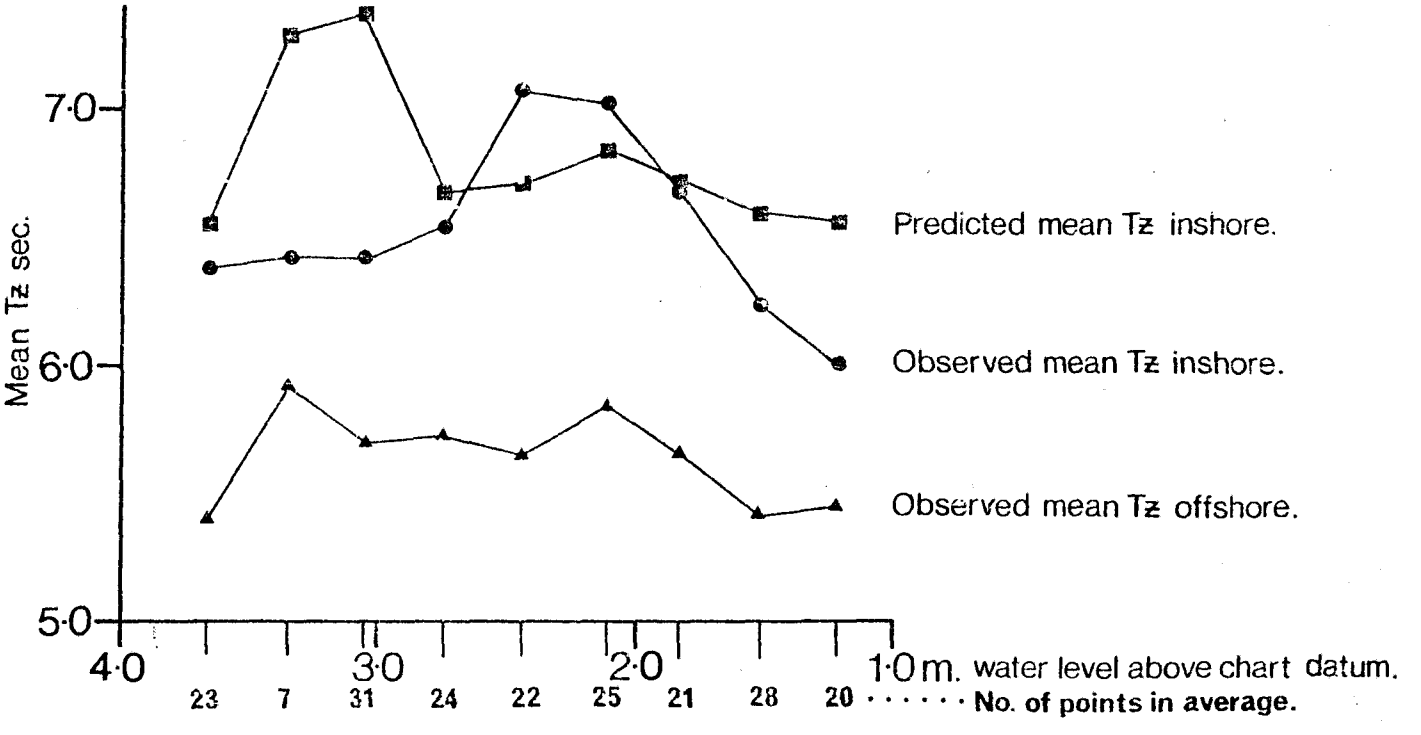

Figure 3 Predicted $H_{\frac{1}{3}}$ and T_z values plotted against observed for a selection of water levels above chart datum. (a) + 3.0m, (b) + 2.44m and (c) + 1.83m.

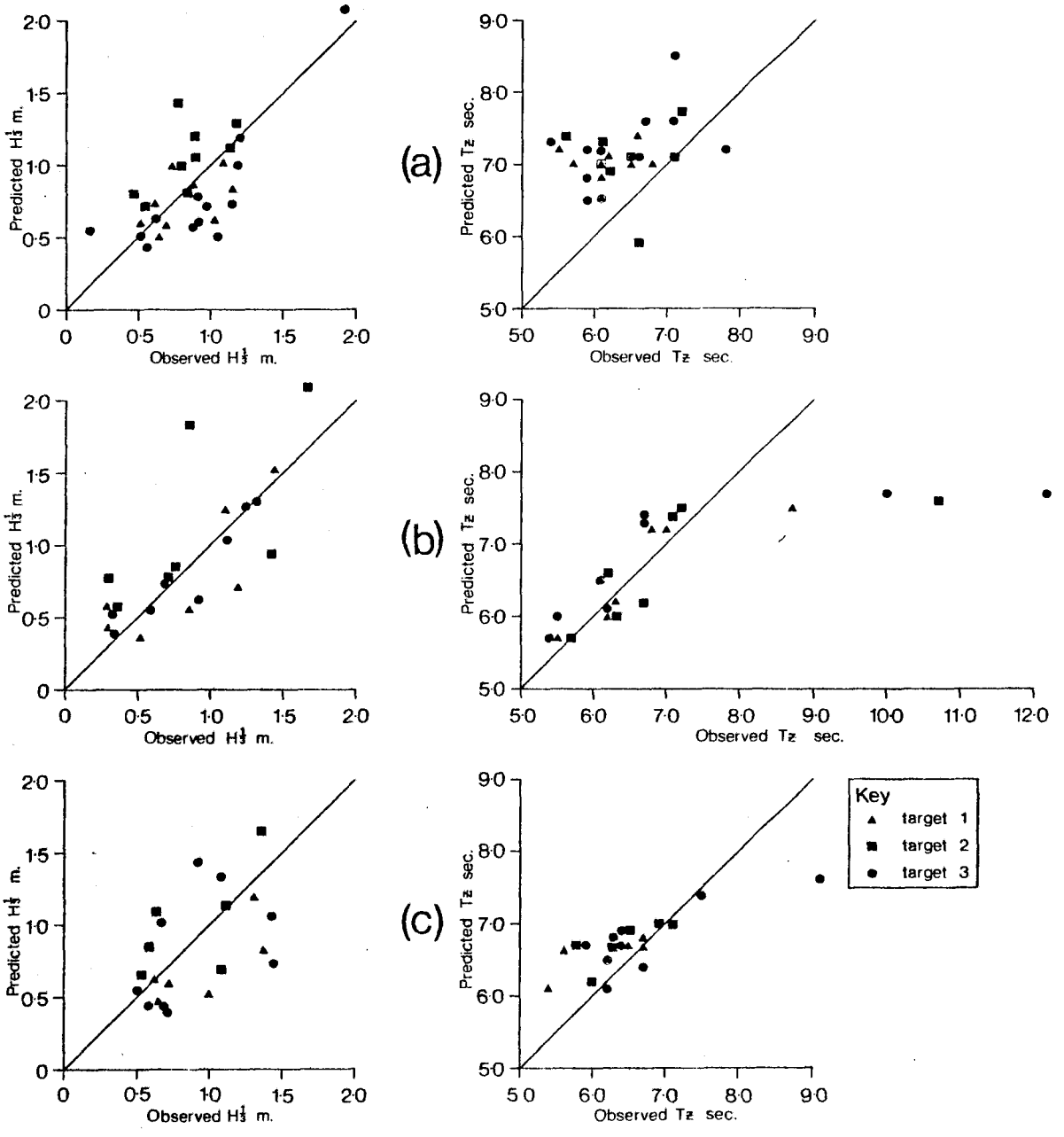

Figure 4: Predicted versus observed $H_{\frac{1}{3}}$ and T_z for Target 1 (Hallsands)

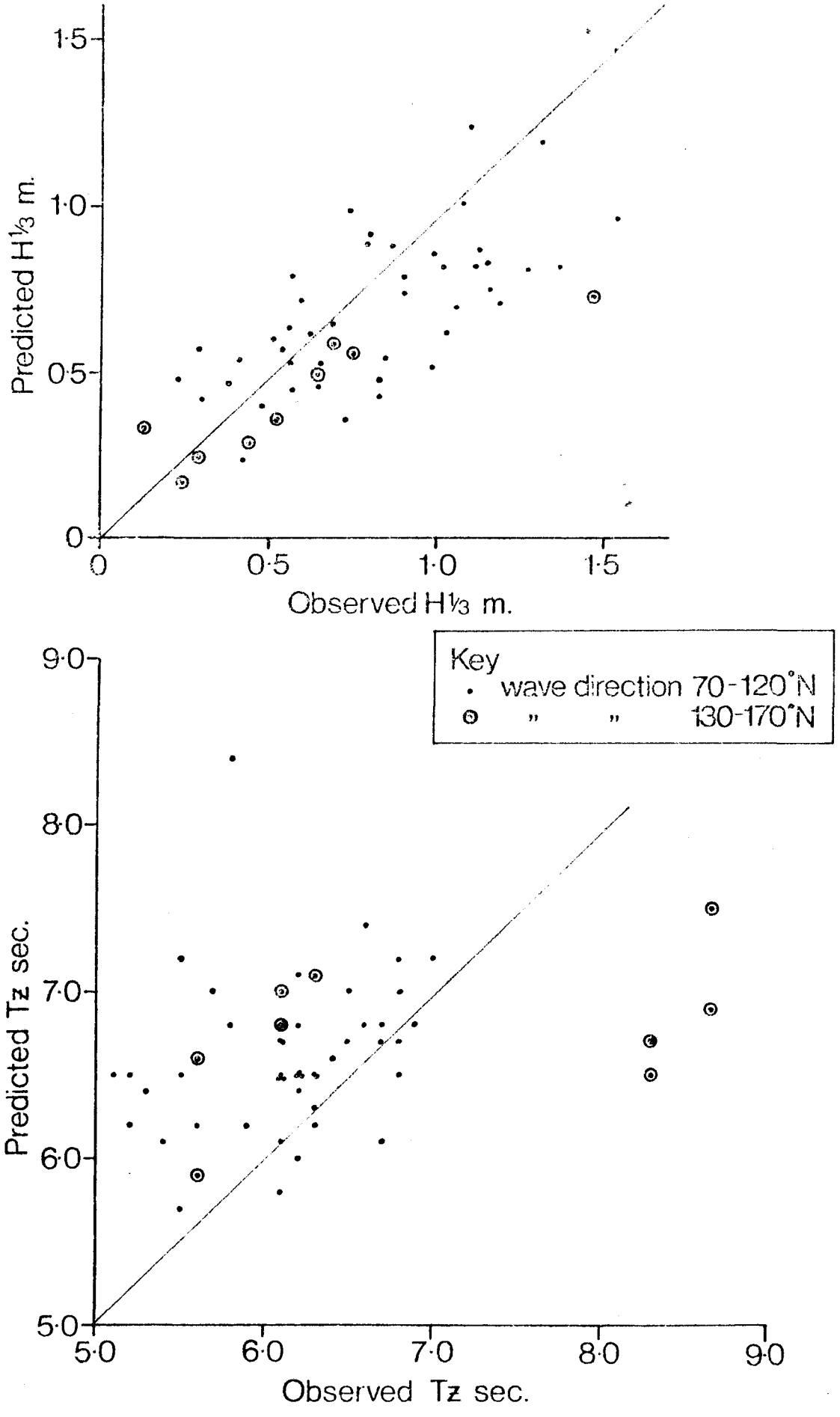

Figure 5 Predicted versus observed $H_{\frac{1}{3}}$ and T_z for Target 2 (Beesands)

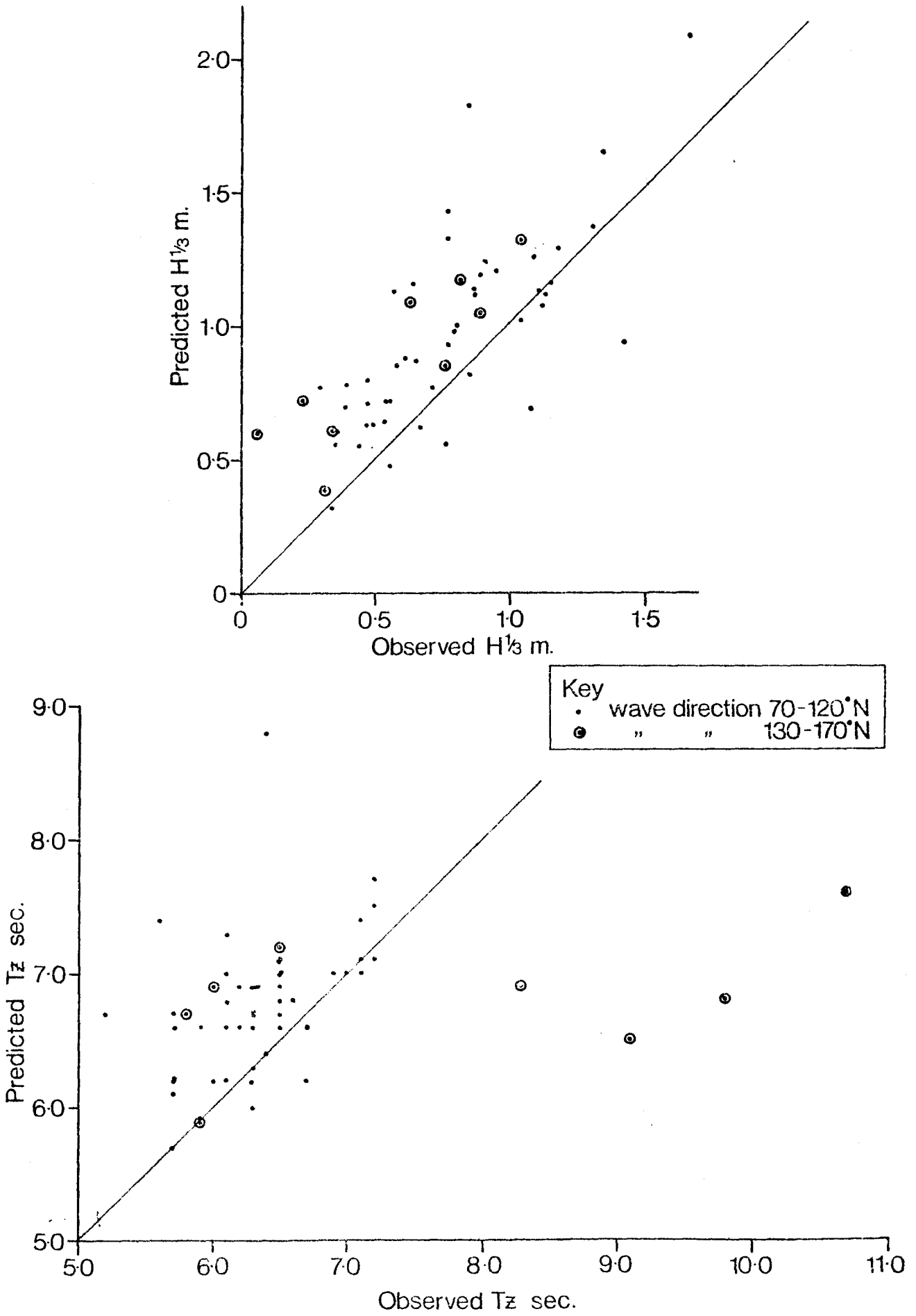

Figure 6 Predicted versus observed $H_{\frac{1}{3}}$ and T_z for target 3 (Slapton)

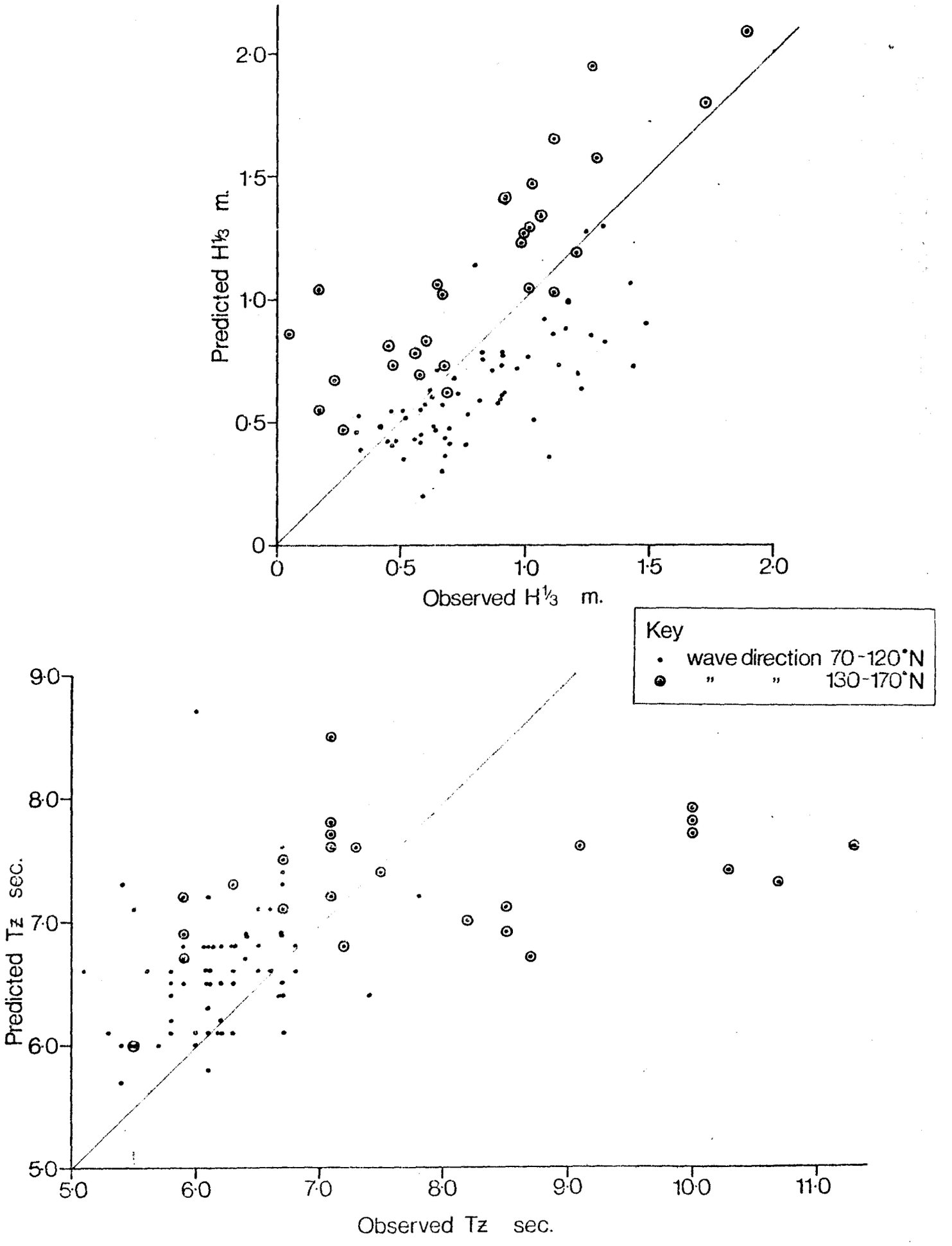

Figure 7 Comparison of 'observed' spectra with their associated Pierson-Moskowitz spectra for some offshore wave records.

Key : ..... Fast Fourier Transform spectrum from digitised wave record. *

——— Pierson-Moskowitz spectrum from $H_{1/3}$ & Tz from the mean rectified wave height & number of zero crossings of the wave record.

- - - - - Pierson-Moskowitz spectrum from $H_{1/3}$ & Tz calculated from the FFT Spectrum.

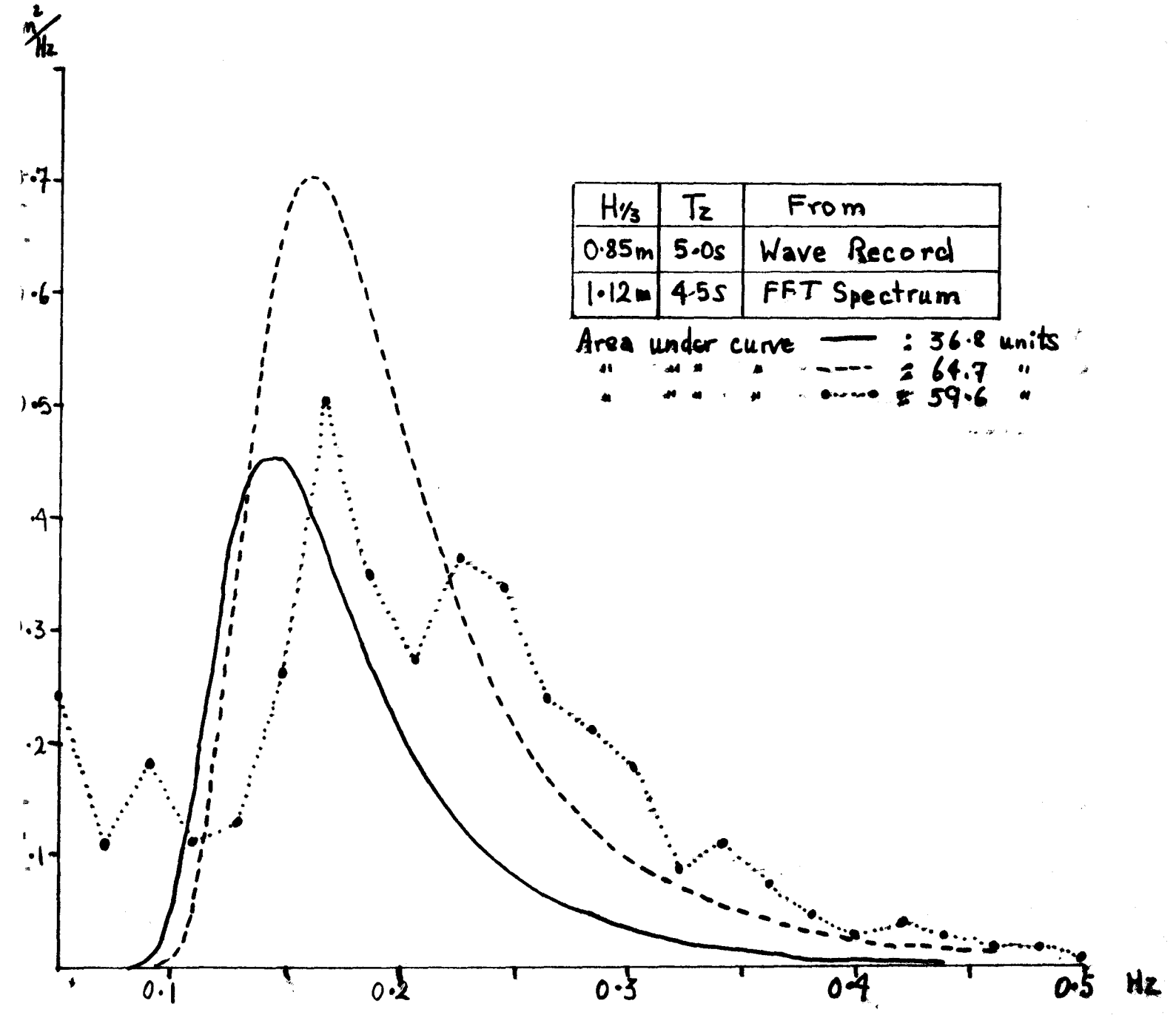

Figure 7 cont'd

* Note: The digitised wave records each consisted of 2048 points. A FFT program was applied seperately to each half (ie 1024 points). The illustrated spectrum was obtained by averaging over 10 points the mean of these two spectra.

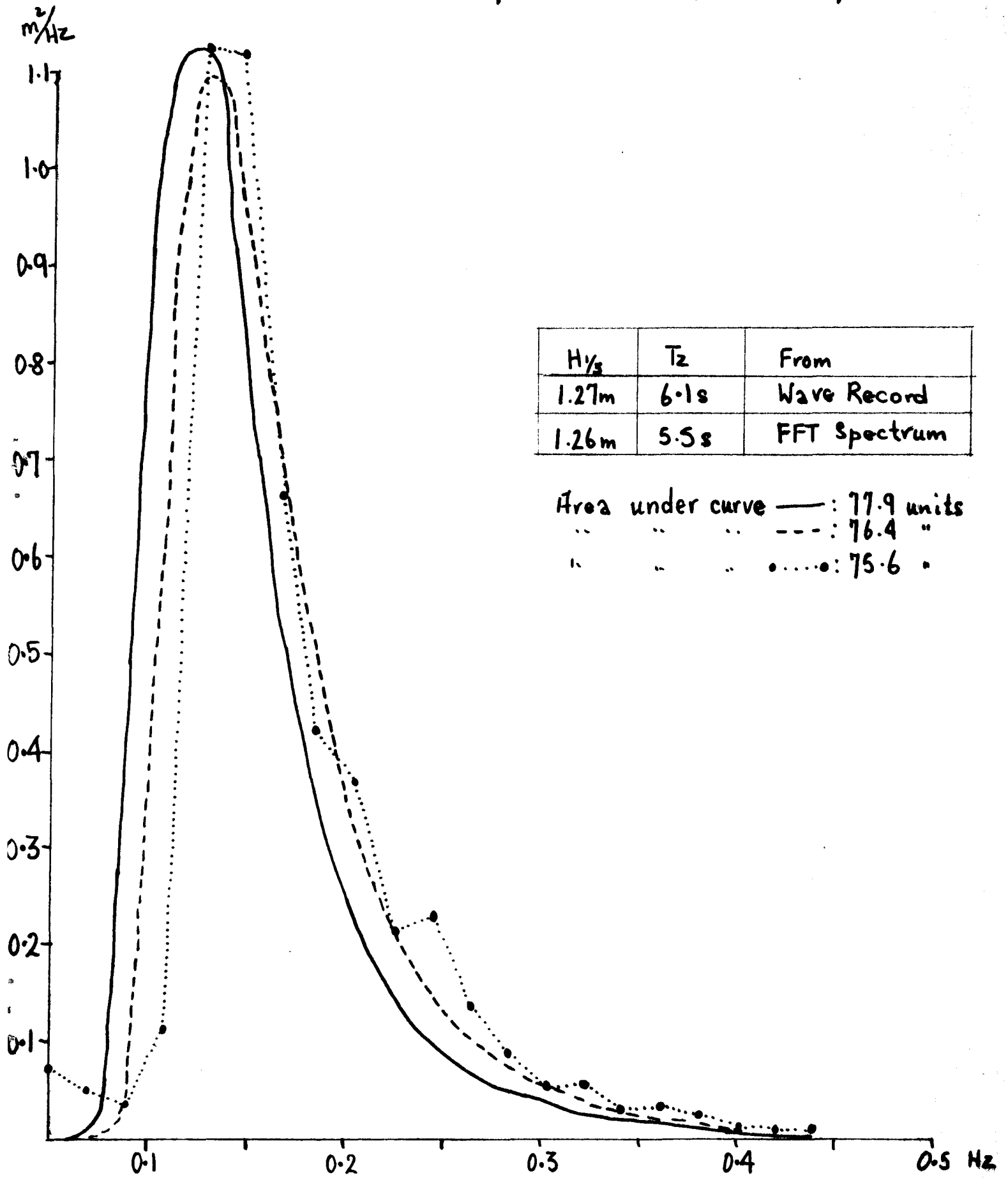

$H_{1/3}$	T_z	From
1.27m	6·1s	Wave Record
1.26m	5·5s	FFT Spectrum

Area under curve ——: 77·9 units
" " " - - -: 76·4 "
" " " •····•: 75·6 "

Figure 7 cont'd

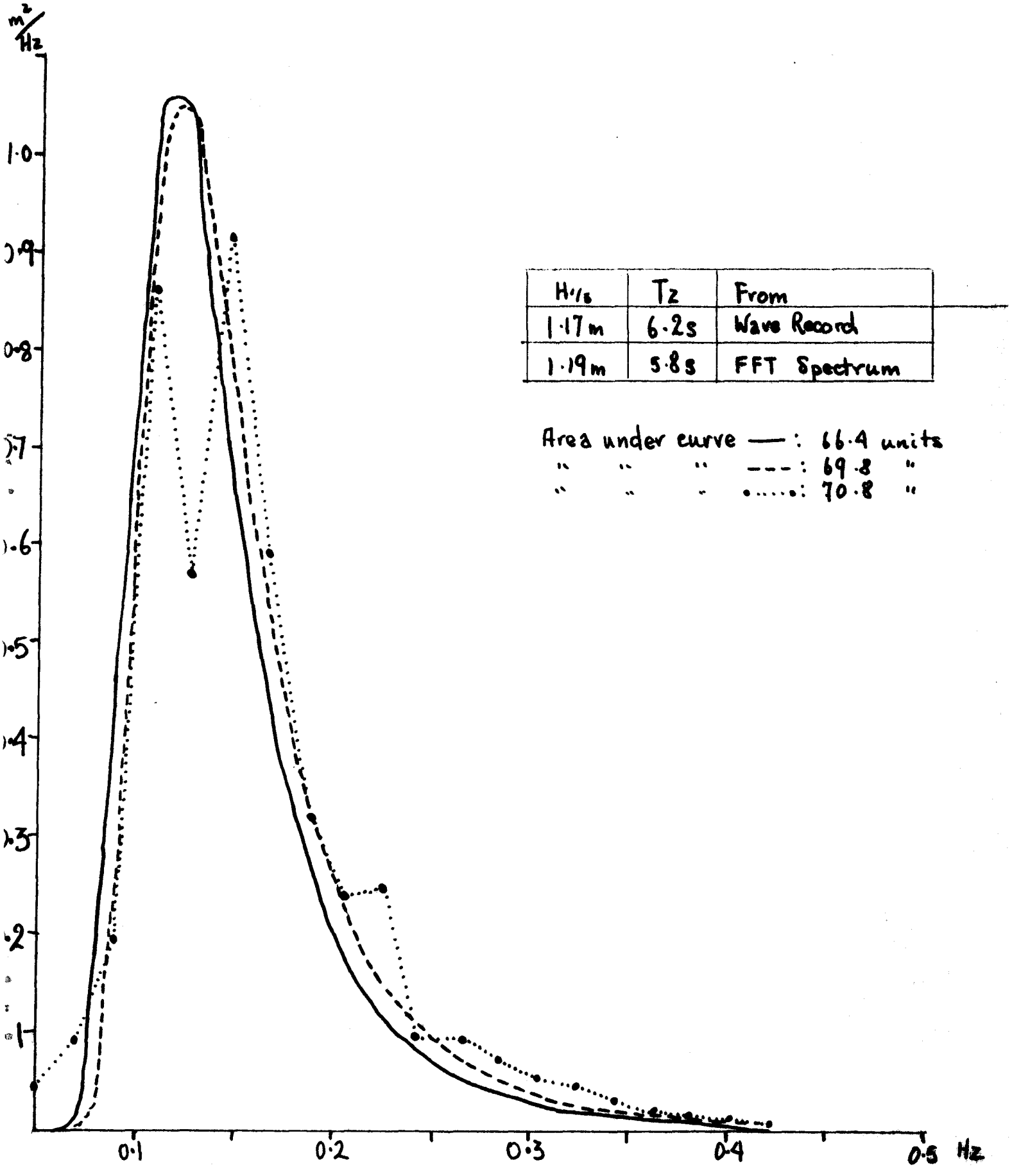

$H_{1/3}$	T_z	From
1·17 m	6·2 s	Wave Record
1·19 m	5·8 s	FFT Spectrum

Area under curve ——: 66·4 units
" " " ---: 69·8 "
" " " •••••: 70·8 "

Figure 7 cont'd.

$H_{1/3}$	Tz	From
0·60m	4·5s	Wave Record
0·60m	4·2s	FFT spectrum

Area under curve —— : 17·7 units
" " " - - - : 17·4 "
" " " •·····•: 17·2 "

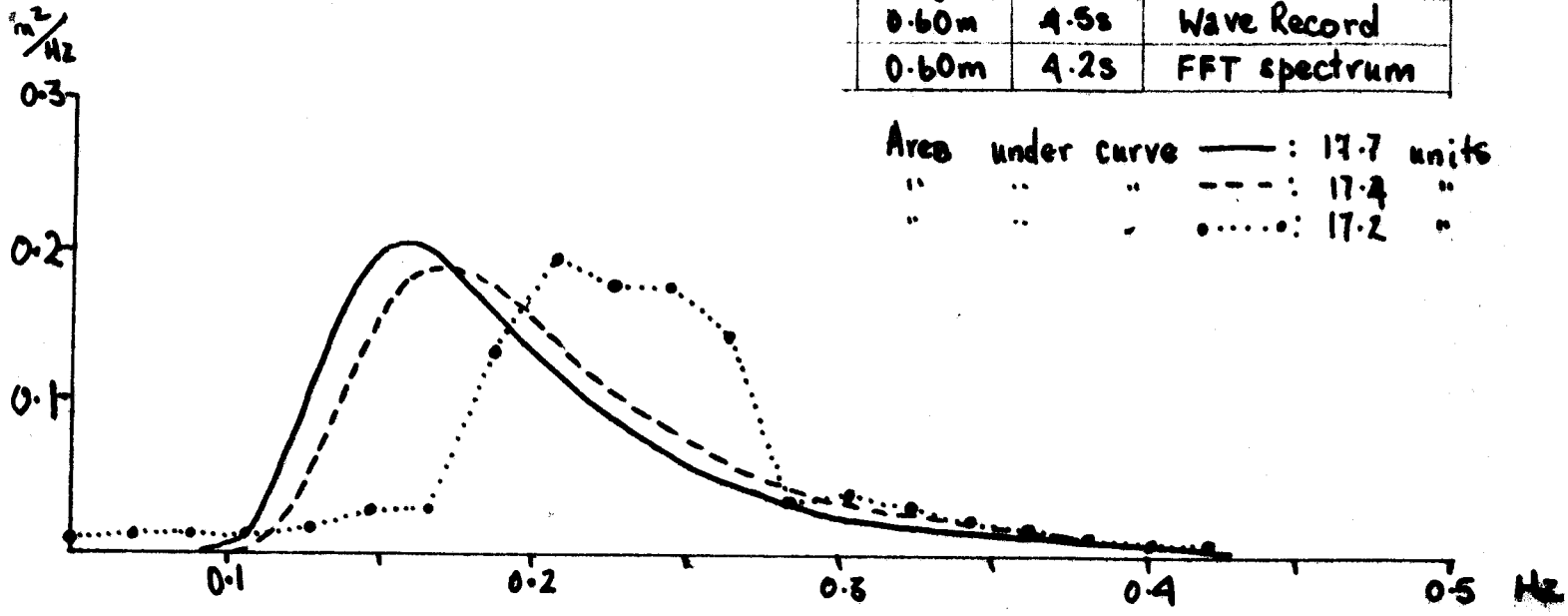

$H_{1/3}$	Tz	From
0·96m	4·8s	Wave Record
1·01m	4·5s	FFT Spectrum

Area under curve —— : 45·9 units
" " " - - - : 51·1 "
" " " •·····• : 51·2 "

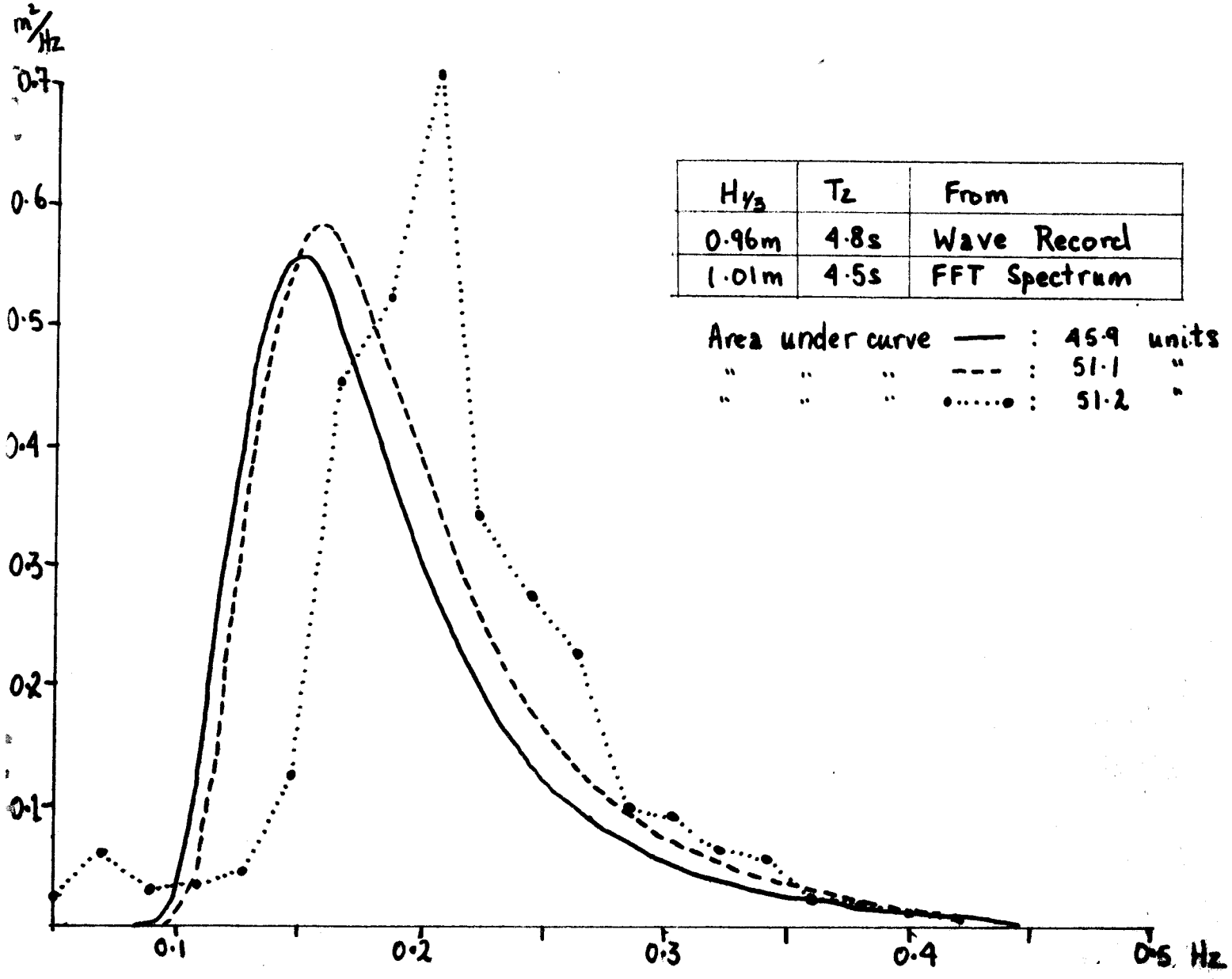

Figure 7 cont'd

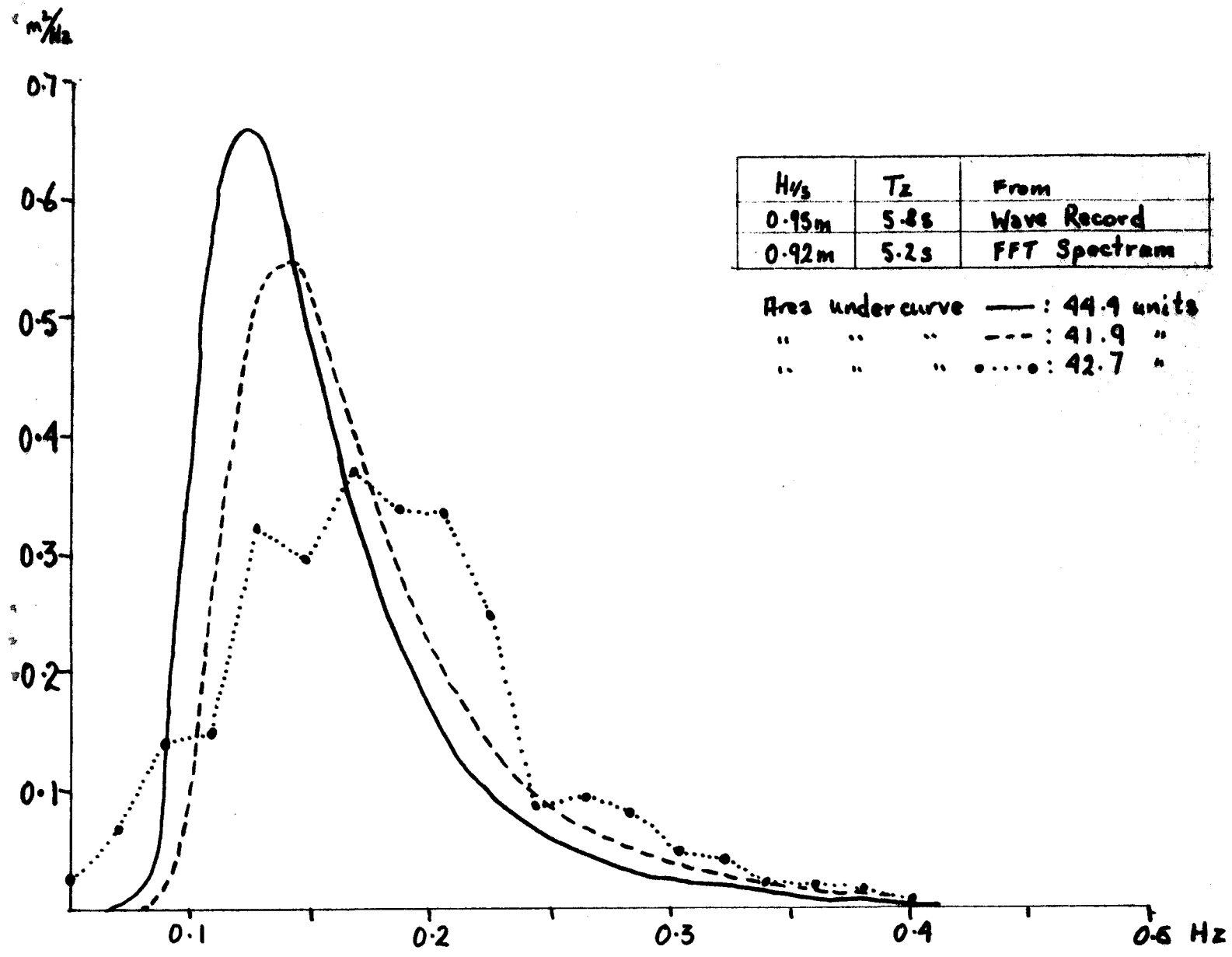

$H_{1/3}$	T_z	From
0·95m	5·8s	Wave Record
0·92m	5·2s	FFT Spectrum

Area under curve ——: 44·9 units
" " " – – –: 41·9 "
" " " •···•: 42·7 "

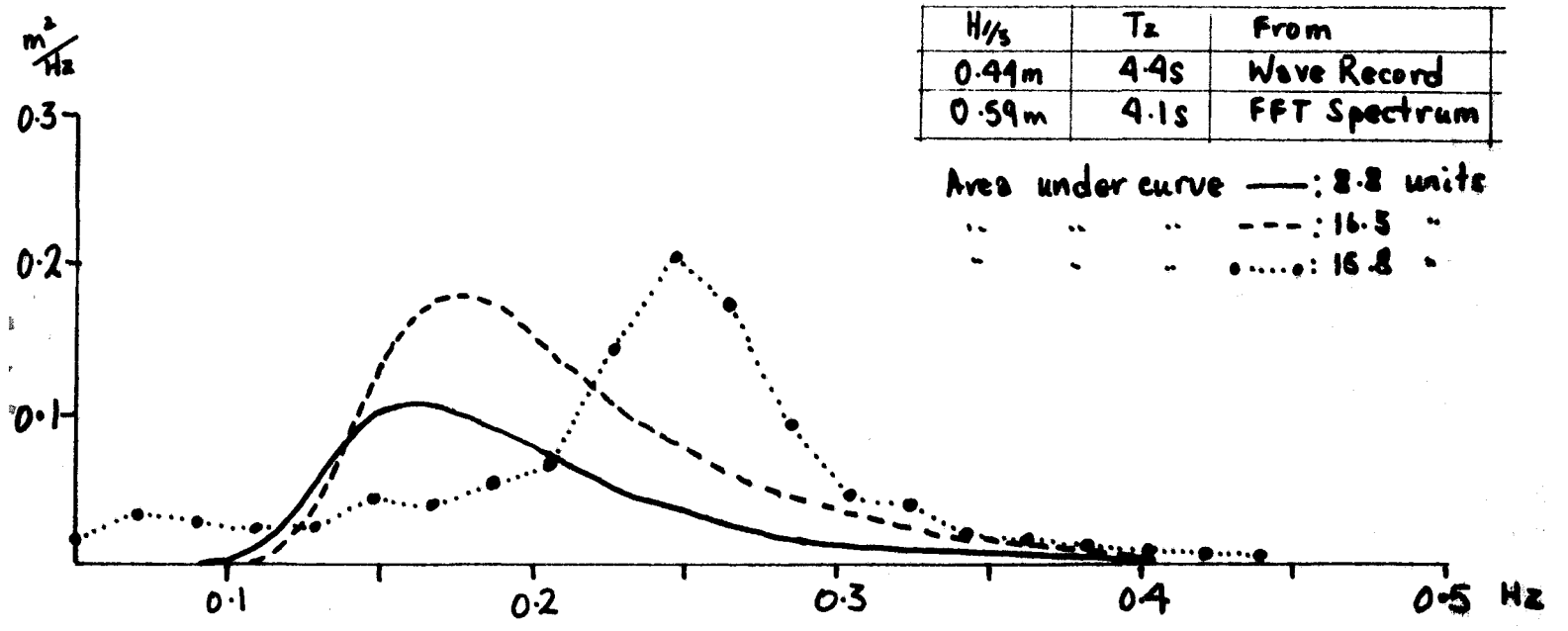

$H_{1/3}$	T_z	From
0·44m	4·4s	Wave Record
0·59m	4·1s	FFT Spectrum

Area under curve ——: 8·8 units
" " " – – –: 16·5 "
" " " •···•: 16·8 "

Figure 7 cont'd

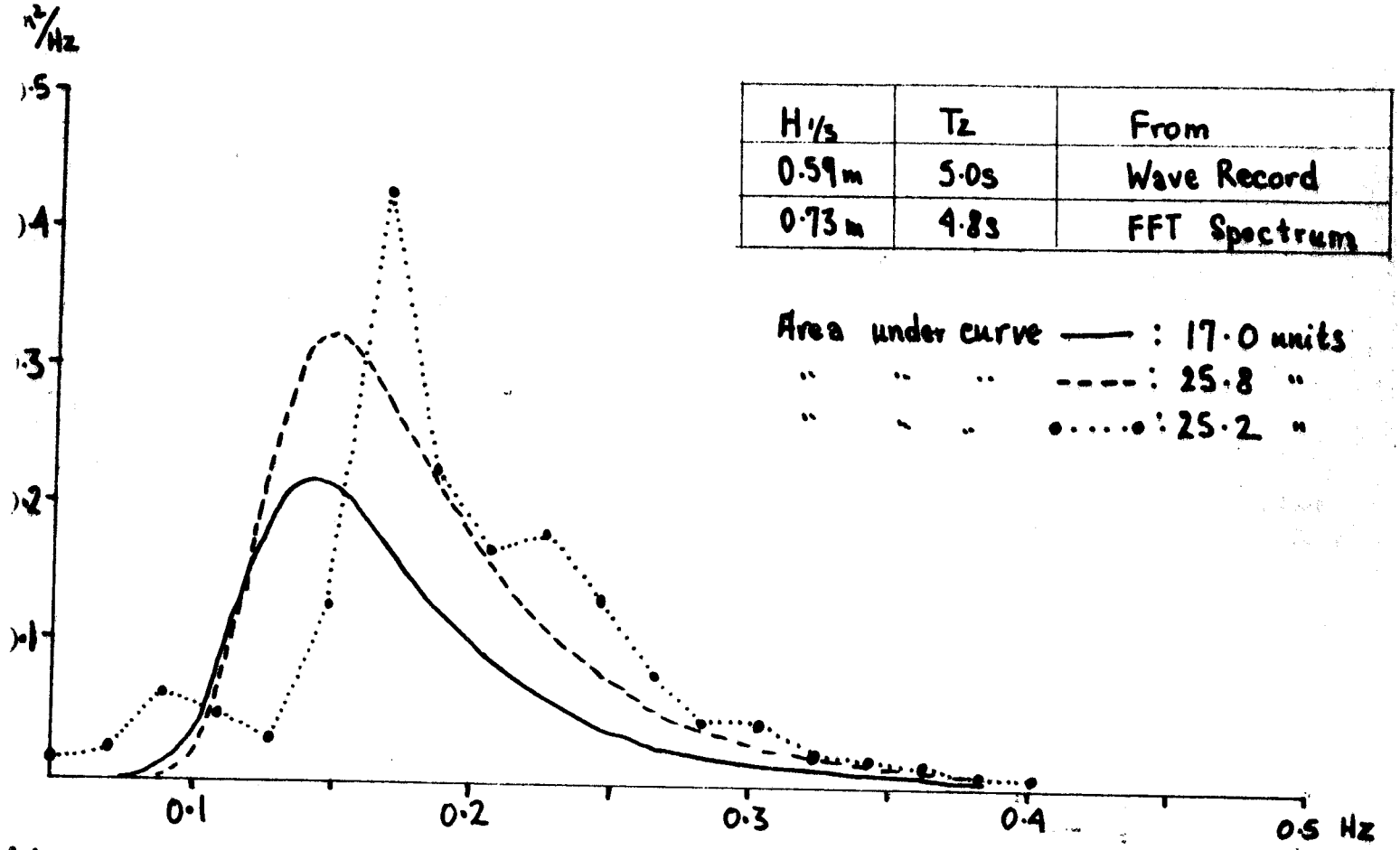

$H_{1/3}$	T_z	From
0·59m	5·0s	Wave Record
0·73m	4·8s	FFT Spectrum

Area under curve —— : 17·0 units
" " " ---- : 25·8 "
" " " •····• : 25·2 "

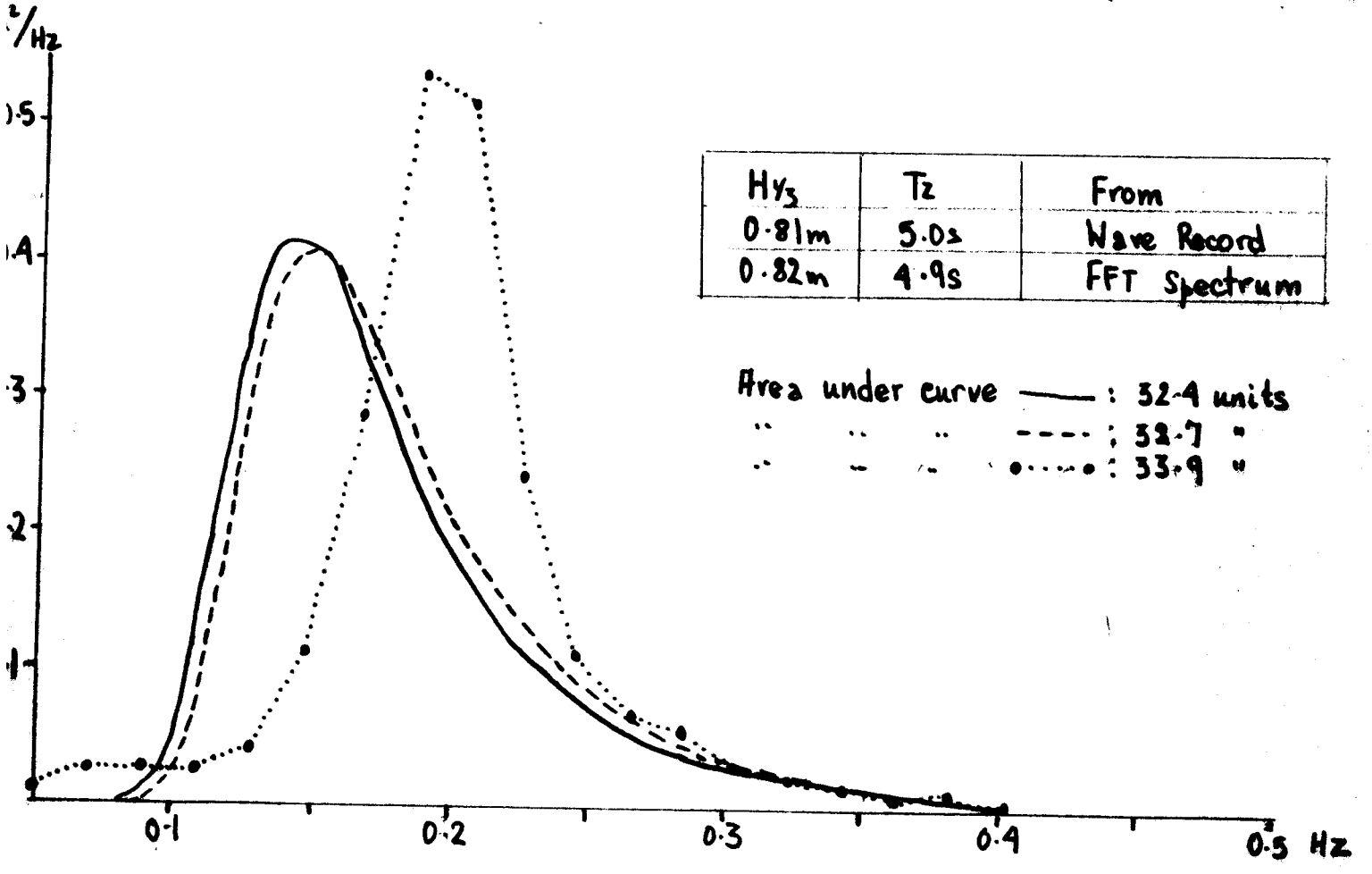

$H_{1/3}$	T_z	From
0·81m	5·0s	Wave Record
0·82m	4·9s	FFT Spectrum

Area under curve —— : 32·4 units
" " " ---- : 32·7 "
" " " •····• : 33·9 "